Laser-Generated Cavitation in Absorbing Liquid Induced by Acoustic Diffraction

M. Frenz*
Institute of Applied Physics, University of Berne, CH-3012 Berne, Switzerland

G. Paltauf and H. Schmidt-Kloiber
Institute of Experimental Physics, Karl-Franzens-University Graz, A-8010 Graz, Austria
(Received 4 March 1996)

Conversion of energy from a heat pulse to acoustic stress is theoretically and experimentally studied in detail. The heat pulse was generated by laser radiation delivered via an optical fiber into an absorbing liquid. The experimental results indicate that tensile stress and cavitation are induced in front of the fiber tip at a distance far below the optical penetration depth of the laser radiation. The occurrence of tensile stress in the acoustic near field of a submerged fiber is explained by acoustic diffraction of the thermoelastic expansion wave. Good agreement between experimental results and theoretical calculations based on a three-dimensional model was found. [S0031-9007(96)00147-0]

PACS numbers: 43.25.+y, 43.30.+m, 79.20.Ds

Cavitation plays an important role in many technical applications such as sonochemistry, lithotripsy, laser surgery in wet fields, bubble chambers, and ultrasonic cleaning. The formation and collapse of cavitation bubbles in liquids are subject for intensive studies since these small bubbles had been made responsible for the destruction of marine propellers. With the development of the laser a new tool for the formation of single, well defined cavitation bubbles in transparent liquids was available. Depending on pulse duration and the wavelength of the laser radiation, three processes for the formation of cavitation bubbles in liquids have been distinguished: plasma induced, due to explosive vaporization, and induced by tensile pressure of an acoustic field.

If a high power laser pulse with a pulse duration shorter than a few nanoseconds is focused into the body of a transparent liquid, optical breakdown is generated at the beam waist due to the high intensity electric field. Caused by the high temperature and pressure the plasma expands initially with hypersonic velocity emitting a shock wave that indicates the conversion of optical energy into mechanical. Additionally, vaporization of water forms a fast expanding cavitation bubble [1–3]. The maximum radius $R_{\max}$ and the lifetime of the bubble T_c are connected by Lord Rayleigh's formula $R_{\max} = T_c/0.915[\rho_0/(p_0 - p_v)]^{1/2}$ whereby ρ_0 is the density of water, p_0 is the hydrostatic pressure, and p_v the vapor pressure inside the bubble [4].

Cavitation can secondly be produced by direct heating and subsequent explosive vaporization of liquid, as in the case of infrared lasers the radiation of which is strongly absorbed by water [6]. The formation of a cavitation bubble at the end of a submerged fiber has recently gained increasing attention as this vapor bubble is used in medical applications to guide IR laser radiation through water [6–8]. This is possible since steam has in contrast to water a low absorption in the IR [9]. Exploiting this effect, tissue can be ablated with IR radiation in a liquid environment even in a noncontact mode as it arises, e.g., in orthopedics, angioplasty, ophthalmology, or lithotripsy.

Tensile stress-induced cavitation and subsequent spallation, i.e., ejection of target material if the amplitude of the tensile stress wave exceeds the tensile strength of the material, is usually generated when a compressive wave is reflected at an impedance mismatched boundary. Spallation was found not only to be the reason for erosion damage of surfaces but also an important mechanism for ablation [10,11]. Strong compressive stress waves are generated in a medium if the energy deposition caused by a short laser pulse is much faster than the thermal expansion of the medium. This situation is called the condition of stress confinement. Reflection of a compressive stress wave at a free boundary (i.e., water-air) changes its sign; the compressive wave becomes a tensile wave. As a result, the stress wave propagating into the target is characterized by a bipolar shape with a leading positive compression wave and a trailing negative tensile wave. If the laser pulse, however, is transmitted to the absorbing medium through a material with higher acoustic impedance (rigid boundary, i.e., glass-water), reflection does not change the sign of the stress wave and the one-dimensional model of thermoelastic stress wave generation does not predict tensile stresses [12,13].

Regardless of the mechanism of formation, the collapse of the cavitation bubble generates a strong pressure transient with an amplitude of up to several kbar that can have strong destructive effects [5,14].

In this study we demonstrate for the first time the generation of tensile stress and cavitation at the end of a submerged fiber tip in liquid (rigid boundary). We experimentally and theoretically show that the tensile stress is induced by diffraction of the acoustic thermoelastic compressive wave at the edge of the fiber. Fast flash Schlieren photography was used to visualize the laser-induced bubble dynamics and the pressure wave propagation produced at a fiber tip in an aqueous dye solution.

 0031-9007/96/76(19)/3546(4)$10.00

In order to efficiently couple thermal energy generated by absorbed laser radiation into mechanical energy, the conditions for thermal and stress confinement have to be satisfied [13,15]. Thermal confinement is fulfilled when the energy deposition occurs on a time scale faster than heat relaxation can take place. This is the case when the pulse duration τ is shorter than the heat diffusion time τ_{th} given by $\tau_{\text{th}} = \delta^2/4\kappa$, where δ is a characteristic length and κ is the thermal diffusivity of the material ($\kappa_{H_2O} = 1.44 \times 10^{-3}$ cm^2/s). If the beam radius is larger than the optical penetration depth, then $\delta = 1/\mu_a$ is the optical penetration depth. When the radius of the laser spot is less than the penetration depth, $\delta = r_{\text{fiber}}$. The radiation conditions fulfill the requirements for stress confinement when τ is shorter than the time τ_{st} ($\tau_{\text{st}} = \delta/c_{\text{water}}$); a stress wave needs to propagate out of the irradiated volume, where δ is again the characteristic length and c_{water} the speed of sound in water.

For the experiments an optical parametric oscillator (OPO) with a tuning range from 400 to 2500 nm was used. Laser pulses (energy $\leq$10 mJ, pulse duration 5–6 ns) were delivered via an optical fiber (600 μm) into an aqueous solution of Orange G which exhibits a high absorption peak at 490 nm to which the OPO was tuned. This resulted in an absorption coefficient of $\alpha = 900$ cm^{-1} of the sample liquid. Time-resolved Schlieren images of stress wave propagation and cavitation in front of the fiber tip were taken with a time-gated video camera using an exposure time of 10 ns. Laser-induced pressure transients were detected using a thin (9 μm) piezoelectric polyvinylidenefluoride (PVDF) foil (rise time of about 4 ns).

Schlieren photographs taken at different times (170 ns, 220 ns, 270 ns, 570 ns, 5 μs, and 50 μs) after the laser pulse are presented in Fig. 1. The heat pulse had a radiant exposure of $H = 1$ J/cm^2 leading to an average computed temperature increase $\Delta T = 147$ °C in a volume below the fiber tip given by the $1/e$ optical penetration depth of the radiation ($\alpha = 900$ cm^{-1}) and the fiber area (not considered latent heat and assuming a constant specific heat capacity). The change in index of refraction generated by the temperature gradient in front of the fiber is seen as a shadow in the Schlieren image (Fig. 1 at 170 ns). This makes the fiber appear longer than it actually is (marked with arrows). The acoustic radiation generated by the heated volume in front of the fiber tip consists of two components. The first is the geometrical wave field component characterized by a plane wave (dark black shadow) conforming to the shape of the fiber. The second component is the boundary diffraction wave field (toroidal wave) that is radiated by the edges of the fiber. In projection, the latter is seen as two dark circles with their center at the edges of the fiber. The images show that cavitation starts at the fiber axis 220 ns after the start of the laser pulse when the diffraction wave field starts to overlap. It is remarkable that the formation of cavitation bubbles in the liquid is locally restricted to the fiber axis. After 570 ns, cavitation extends to a depth

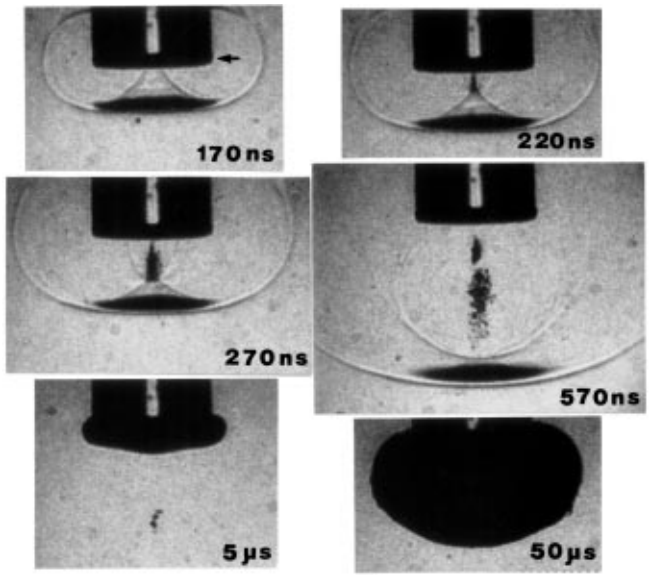

FIG. 1. Schlieren images of stress wave propagation and cavitation in aqueous dye solution taken at different times after laser pulse delivery ($H = 1$ J/cm^2, $\alpha = 900$ cm^{-1}, fiber diameter $D = 600$ μm). The position of the end of the fiber is marked by an arrow in the first image.

of about 550–600 μm below the fiber tip, a distance much larger than the optical penetration depth $1/\alpha = 11$ μm of the radiation. In contrast to the cavitation bubbles, a thermal or vaporization bubble is formed (after 5 μs) directly attached to the fiber surface. It reaches its maximum extension at $\sim$50 μs and collapses after about 100 μs. During the collapse a strong pressure transient is generated [5].

The theoretical calculations of the laser-induced acoustic field are based on the general solution of the wave equation in a liquid [16]. To derive the solution of the wave equation from an initial thermoelastic stress distribution, the following assumptions were made: (i) the spatial beam profile of the laser at the fiber tip is a "top-hat" profile with an exponential decay of the radiation outside the fiber, (ii) the initial pressure distribution which is generated by instantaneous deposition of the laser energy has an exponential decay in direction of the fiber axis, and (iii) the reflection of the acoustic wave at the water-fiber surface was taken into account by adding an image pressure distribution at $-z$. To derive the general solution of the acoustic wave equation in three dimensions we used the Poisson formula [16,17] which yields the velocity potential ψ at any time and position in space if initial values of the potential ψ_0 and its first time derivative are known:

$$\psi(x,y,z,t) = \frac{1}{4\pi}\left[\frac{\partial}{\partial t}\left(t\int \psi_0|_{R=ct}\,do\right) + t\int \dot{\psi}_0|_{R=ct}\,do\right]. \quad (1)$$

do is the surface element on the unit sphere. The subscript $R = ct$ means that the values of ψ_0 and $\dot{\psi}_0$ are taken on a sphere with radius R around the point (x, y, z). Since

instantaneous energy deposition leads to an initial pressure rise without any material displacement in the target, the first integral in (1) becomes zero. The relation between the pressure and the velocity potential is given by

$$p = -\rho\, \partial\psi/\partial t\,, \tag{2}$$

where ρ is the density. Therefore the second integral in (1) contains essentially the initial pressure distribution $p_0(r,z) = \alpha\Gamma H_0 e^{-\alpha z} f(r)$, with α the absorption coefficient, Γ the Grüneisen coefficient, and H_0 the incident radiant exposure. The function $f(r)$ describes the spatial profile of the laser beam $f(r) = 1$ for $r \le a$ and $f(r) = e^{-(r-a)^2/d^2}$ for $r > a$. The variable z describes the distance between the fiber tip and the observation point. The Grüneisen coefficient is defined by $\Gamma = \beta/\rho C_V \kappa_T$, with β the thermal expansion coefficient, C_V the specific heat at constant volume, and κ_T the isothermal compressibility ($\Gamma_{\text{water}} = 0.11$ at room temperature).

The positive and negative amplitudes of the normalized pressure field $p^*(r,z,t) = p(r,z,t)/\alpha\Gamma H_0$ obtained after numerical evaluation of Eqs. (1) and (2) are shown in Fig. 2 as a function of r for a constant value of $z = 100$ μm (fiber diameter $D = 600$ μm, $\alpha = 900$ cm^{-1}). The calculations reveal a constant positive compression pressure over almost the entire fiber diameter (seen in Fig. 1, image after 170 ns as a plane wave) and a sharp maximum of the tensile stress at the fiber axis generated by the diffraction wave field.

The temporal behavior of the pressure signal calculated with the three-dimensional model at the fiber axis ($r = 0$) for a distance of $z = 100$ μm shows that the negative pressure transient has a delay of about 160 ns with respect to the positive which is equal to the propagation time from the edge of the fiber to the observation point [Fig. 3(a), $z = 100$ μm]. This is in good agreement with the visual observation (Fig. 1) that tensile stress-induced cavitation does not begin unless the rarefraction wave generated at the edges of the fiber has arrived at the fiber axis. Since the difference in propagation time between waves originating at the edge of the disk and at the center decreases with increasing observation coordinate z, the delay between both components also decreases resulting in a symmetric, bipolar wave form [Fig. 3(a), $z = 6.5$ mm]. This change in the temporal behavior of the pressure signal reflects the transition between acoustical near and far field. Assuming a scalar wave theory and, further, that the dimension of the acoustic source is large compared to the acoustic wavelength, then the distance z_f where the border between acoustic near field and far field is located is defined as $z_f = D^2\alpha/8$ [18,19]. Hence, for an absorption coefficient $\alpha = 900$ cm^{-1}, a fiber diameter $D = 600$ μm, and a pulse duration $\tau = 6$ ns the transition from the near to the acoustic far field is located at $z_f = 4$ mm. In this theory, the diffraction of a circular acoustic source is modeled by assuming that the acoustic wave is well confined within a cylinder of diameter D up to a distance

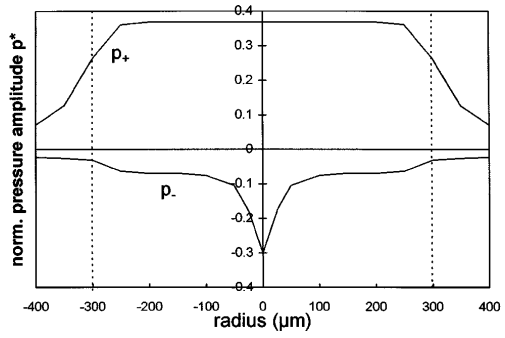

FIG. 2. Positive (p_+) and negative (p_-) stress amplitudes as a function of the radius r, calculated for a distance of $z = 100$ μm from the fiber tip. The dashed lines indicate the fiber diameter ($D = 600$ μm).

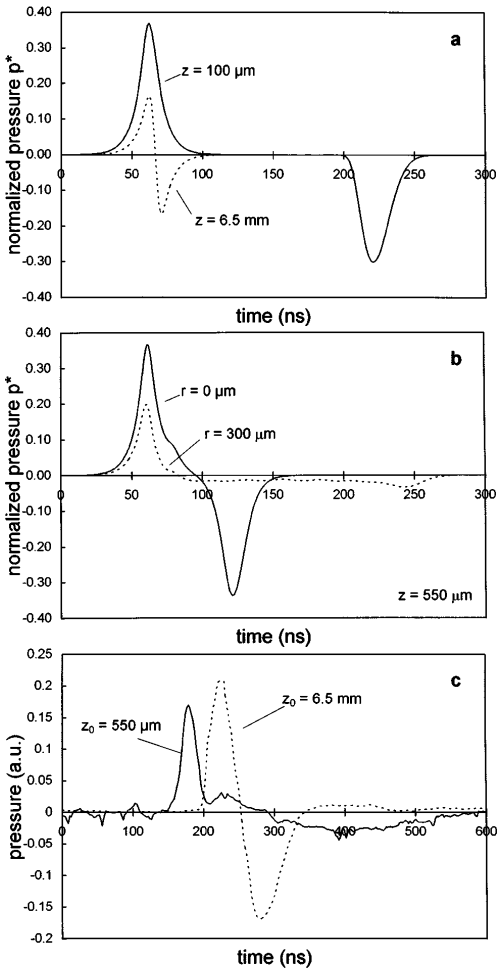

FIG. 3. Calculated (three-dimensional model) and measured stress signals caused by a 6 ns laser pulse ($D = 600$ μm, $\alpha = 900$ cm^{-1}). The time scale does not reflect the actual propagation time of the pressure signal with respect to the laser pulse. (a) Calculated in the near field $z = 100$ μm and in the far field $z = 6.5$ mm. (b) Calculated at a distance of $z = 550$ μm at the fiber axis $r = 0$ μm and off-axis $r = 300$ μm. (c) Measured in the near field $z = 550$ μm and in the far field $z = 6.5$ mm. Both measurements were done with a piezoelectrical detector (PVDF foil) of 2 mm diameter.

z_f; thereafter it diverges spherically into a cone with apex angle $2\Theta_T = 2\arcsin(D/2z_f)$, and with the apex centered in the center of the source. The scalar wave theory shows that the initial plane wave for $z < z_f$ becomes a spherical wave for $z > z_f$. This theory hence only one dimensional does not predict the strong tensile stress on the fiber axis in the acoustic near field.

Figure 3(b) shows stress signals calculated at a distance $z = 550$ μm at the fiber axis $r = 0$ μm and off-axis $r = 300$ μm. The tensile stress amplitude is much higher on the symmetry axis than off-axis which again shows that a maximum of tensile stress is generated at the fiber axis (compare to Fig. 2).

The stress signals measured with the PVDF-pressure transducer at variable observation distances are shown in Fig. 3(c). Whereas experiments and theory agree well in the far field [Figs. 3(a) and 3(c)], there is a discrepancy in the calculated and measured signals at the fiber axis ($r = 0$) in the near field. The reason for this discrepancy is the relatively large area (diameter = 2 mm) of the pressure transducer used which does not provide the required spatial resolution. The detector integrates the incoming stress wave over its active area and most of the detector records off-axis ($r > 0$) signals like the one calculated for $r = 300$ μm [see Fig. 3(b)], whereas the calculation gives the stress at a certain point. The dimension of the detector is also the reason for the larger pressure amplitude measured in the far field than in the near field [see Fig. 3(c)].

The comparison between the measured and calculated pressure transients and the simultaneously recorded Schlieren images clearly show that even when the condition for plane wave propagation is satisfied (beam diameter $D \gg \delta$), tensile stress-induced cavitation bubbles can be created in the acoustic near field of a submerged fiber. The calculation of the amplitudes of compression and rarefraction pressure waves as a function of the distance to the fiber axis [Figs. 3(a) and 3(b)] verifies that for the parameter set used the rarefraction wave is essentially located at the fiber axis (see Fig. 1, $t = 570$ ns). The conditions are comparable to those below an air-water boundary where a laser-induced compressive wave is reflected with negative sign due to the acoustical impedance mismatch although the tensile stress at a "free" surface is almost constant over the entire beam diameter [11]. In this study we have shown for the first time that the creation of tensile stress in the acoustic near field of a submerged fiber tip is caused by diffraction of the acoustic plane wave at the fiber edges.

Since the fracture threshold of a material is much lower for tensile stress than for compressive stress, the findings of this study are of importance for all applications where short fiber delivered laser pulses are used. For example, using short fiber delivered laser pulses for minimally invasive laser surgery, the mechanical strength of the tissue might be drastically lowered by the tensile stress generated at the fiber tip that is in direct contact with tissue. This mechanical process can explain why the experimentally determined threshold for tissue ablation is almost an order of magnitude lower than the theoretically calculated energy density need for vaporization [20]. Moreover, the change of the mechanical tissue properties and thereby induced mechanical tissue damage can affect a much larger volume than that determined by the optical penetration depth of the radiation.

In summary, we have studied the onset of cavitation bubble formation at a fiber tip submerged in an absorbing liquid. The theory and experiment show that tensile stress-induced cavitation is created in the acoustic near field of the fiber. The occurrence of tensile stress is shown to arise from acoustic diffraction of the thermoelastic stress wave at the finite size of the fiber.

This work was supported by the Austrian Science Foundation FWF (Projects P8886 and P10769 Med) and by the Swiss Commission for the Encouragement of Scientific Research.

*Electronic address: frenz@iap.unibe.ch

[1] V. S. Teslenko, Sov. J. Quantum Electron. **7**, 981 (1977).
[2] A. Vogel *et al.*, Lasers Surg. Med. **15**, 32 (1994).
[3] J. G. Fujimoto *et al.*, Invest. Ophthalmol. Vis. Sci. **26**, 1771 (1985).
[4] O. M. Lord Rayleigh, Philos. Mag. **34**, 94 (1917).
[5] M. Frenz *et al.*, in *Biomedical Optics, Laser-Tissue-Interaction V*, edited by S. L. Jacques and A. Katzir (SPIE, Bellingham, 1994), Vol. 2134, p. 402.
[6] H. Pratisto *et al.*, Appl. Phys. Lett. **67**, 1963 (1995).
[7] T. G. van Leeuwen *et al.*, Lasers Surg. Med. **11**, 26 (1991).
[8] M. Ith *et al.*, Appl. Phys. B **59**, 621 (1994).
[9] K. L. Vodopyanov, Sov. Phys. JETP **70**, 114 (1990).
[10] R. S. Dingus and B. P. Shafer, in *Laser-Tissue Interaction I*, edited by S. L. Jacques and A. Katzir (SPIE, Bellingham, 1990), Vol. 1202, p. 36.
[11] G. Paltauf and H. Schmidt-Kloiber, Lasers Surg. Med. **16**, 227 (1995).
[12] E. F. Carome, N. A. Clark, and C. E. Moeller, Appl. Phys. Lett. **4**, 95 (1964).
[13] J. C. Bushnell and D. J. McCloskey, J. Appl. Phys. **39**, 5541 (1968).
[14] A. Vogel, W. Lauterborn, and R. Timm, J. Fluid Mech. **206**, 299 (1989).
[15] S. L. Jacques, Surg. Clin. North Am. **72**, 531 (1992).
[16] L. D. Landau and E. M. Lifschitz, *Hydrodynamic* (Akademie, Berlin, 1981).
[17] G. Paltauf, M. Frenz, and H. Schmidt-Kloiber, in *Laser-Tissue-Interaction and Tissue Optics*, edited by M. J. C. van Gemert, R. W. Steiner, L. O. Svaasand, H. J. Albrecht, and A. Katzir (SPIE, Bellingham, 1995), Vol. 2624, p. 72.
[18] V. M. Ristic, *Principles of Acoustic Devices* (John Wiley & Sons, New York, 1983).
[19] M. W. Sigrist, J. Appl. Phys. **60**, R83 (1986).
[20] D. Albagli *et al.*, Lasers Life Sci. **6**, 55 (1994).